IOP Conf. Series: Journal of Physics: Conf. Series **800** (2017) 012002 doi:10.1088/1742-6596/800/1/012002

LHCb searches for the strong CP-violating decays $\eta\to\pi\pi$ and $\eta'\to\pi\pi$

L Capriotti, on behalf of the LHCb Collaboration

School of Physics and Astronomy, The University of Manchester, Oxford Road, Manchester M13 9PL, United Kingdom

E-mail: lorenzo.capriotti@postgrad.manchester.ac.uk

Abstract. A search for the CP-violating strong decays $\eta \to \pi^+\pi^-$ and $\eta'(958) \to \pi^+\pi^-$ has been performed using approximately 2.5×10^7 events of each of the decays $D^+ \to \pi^+\pi^+\pi^-$ and $D_s^+ \to \pi^+\pi^+\pi^-$, recorded by the LHCb experiment. The data set corresponds to an integrated luminosity of $3.0\,\text{fb}^{-1}$ of pp collision data recorded during LHC Run 1 and $0.3\,\text{fb}^{-1}$ recorded in Run 2. No evidence is seen for $D^+_{(s)} \to \pi^+\eta^{(\prime)}$ with $\eta^{(\prime)} \to \pi^+\pi^-$, and upper limits at 90% confidence level are set on the branching fractions, $\mathcal{B}(\eta \to \pi^+\pi^-) < 1.6 \times 10^{-5}$ and $\mathcal{B}(\eta' \to \pi^+\pi^-) < 1.8 \times 10^{-5}$. The limit for the η decay is comparable with the existing one, while that for the η' is a factor of three smaller than the previous limit.

1. Introduction

The strength of *CP* violation in weak interactions in the quark sector is well below what would be required to serve as an explanation for the observed imbalance between the amounts of matter and antimatter in the universe. The QCD Lagrangian could contain a term, the θ term [1], that would give rise to *CP* violation in strong interactions; however, no strong *CP* violation has been observed. This apparent absence of *CP* violation in QCD is known as the "strong *CP* problem".

2. The strong *CP* problem

The strong *CP* problem arises from the structure of the degeneracy of the vacuum in QCD [2,3]. The QCD vacuum has, in fact, a periodic structure; the true vacuum state, called θ-vacuum, is obtained as a superposition of all the vacuum states:

$$|\theta\rangle = e^{in\theta}\,|n\rangle\,.$$

When calculating vacuum to vacuum transitions, using the θ vacuum as true vacuum of the theory, an extra term in the QCD Lagrangian appears, called the "θ term",

$$\mathcal{L}_\theta = \theta\frac{g_s^2}{64\pi^2}\epsilon_{\mu\nu\alpha\beta}F_a^{\mu\nu}F_a^{\alpha\beta},$$

which violates *CP*. The experimental upper limit on the neutron electric dipole moment (nEDM) implies a limit $\theta \lesssim 10^{-10}$ [4]. The closeness of the value of θ to zero is seen as a fine-tuning problem of the theory.

Content from this work may be used under the terms of the Creative Commons Attribution 3.0 licence. Any further distribution of this work must maintain attribution to the author(s) and the title of the work, journal citation and DOI.
Published under licence by IOP Publishing Ltd

3. The $\eta^{(\prime)} \to \pi^+\pi^-$ decays

The decay modes $\eta \to \pi^+\pi^-$ and $\eta'(958) \to \pi^+\pi^-$ would both violate *CP* symmetry. In the Standard Model (SM) these decays could happen via the *CP*-violating weak interaction, through mediation by a virtual K^0_S meson, with expected branching fractions $\mathcal{B}(\eta \to \pi^+\pi^-) < 2 \times 10^{-27}$ and $\mathcal{B}(\eta' \to \pi^+\pi^-) < 4 \times 10^{-29}$ [5]. Based on the limit from the nEDM measurements, strong decays mediated by the θ term would have branching fractions below about 3×10^{-17} [5]. Any observation of larger branching fractions would indicate a new source of *CP* violation in the strong interaction. The current best limit for the $\eta \to \pi^+\pi^-$ decay mode, $\mathcal{B}(\eta \to \pi^+\pi^-) < 1.3 \times 10^{-5}$ at 90% confidence level (CL), is obtained from the KLOE experiment [6], which looked for $\eta \to \pi^+\pi^-$ in the decay $\phi(1020) \to \eta\gamma$. The limit for η', $\mathcal{B}(\eta' \to \pi^+\pi^-) < 5.5 \times 10^{-5}$ at 90% CL, is from the BESIII experiment [7], based on searches for $\eta' \to \pi^+\pi^-$ in radiative $J/\psi \to \eta'\gamma$ decays. In the study presented here, a new method is introduced to search for the decays $\eta \to \pi^+\pi^-$ and $\eta' \to \pi^+\pi^-$, exploiting the large sample of charm mesons collected by LHCb; any contribution would show as narrow peaks, consistent with mass resolution, in the inclusive $\pi^+\pi^-$ mass spectra.

4. Analysis strategy at LHCb

In the analysis [8], the decays $D^+ \to \pi^+\pi^+\pi^-$ and $D^+_s \to \pi^+\pi^+\pi^-$ are used to look for the presence of η and η' resonances in the $\pi^+\pi^-$ mass spectra, which could come from the known decays $D^+_{(s)} \to \pi^+\eta^{(\prime)}$ (inclusion of charge-conjugate modes is implied throughout). The data samples comprise about 25 million each of $D^+ \to \pi^+\pi^+\pi^-$ and $D^+_s \to \pi^+\pi^+\pi^-$ decays, from integrated luminosities of $3.0\,\text{fb}^{-1}$ of pp collision data recorded by LHCb in LHC Run 1 and $0.3\,\text{fb}^{-1}$ recorded in 2015 during Run 2. The data from Run 2 correspond to a 10% increase in integrated luminosity, but a 30% increase in number of signal candidates. They are processed through the Turbo stream, which performs an online reconstruction of candidates with offline quality, removing the need for any additional offline reconstruction [9].

For $N(\eta^{(\prime)})$ observed $\eta^{(\prime)}$ signal decays in the $\pi^+\pi^-$ mass spectrum from a total of $N(D^+_{(s)})$ mesons reconstructed in the $\pi^+\pi^+\pi^-$ final state, the measured branching fraction would be

$$\mathcal{B}\left(\eta^{(\prime)} \to \pi^+\pi^-\right) = \frac{N(\eta^{(\prime)})}{N(D^+_{(s)})} \times \frac{\mathcal{B}(D^+_{(s)} \to \pi^+\pi^+\pi^-)}{\mathcal{B}(D^+_{(s)} \to \pi^+\eta^{(\prime)})} \times \frac{1}{\epsilon(\eta^{(\prime)})}\,, \tag{1}$$

where $\epsilon(\eta^{(\prime)})$ is a small correction that accounts for any variation of efficiency with $\pi^+\pi^-$ mass. The values of $N(D^+_{(s)})$ and $N(\eta^{(\prime)})$ and their uncertainties are obtained from fits to the $\pi^+\pi^-\pi^+$ and $\pi^+\pi^-$ mass spectra of the selected $D^+_{(s)} \to \pi^+\pi^+\pi^-$ candidates; the branching fractions $\mathcal{B}(D^+_{(s)} \to \pi^+\pi^+\pi^-)$ and $\mathcal{B}(D^+_{(s)} \to \pi^+\eta^{(\prime)})$ and their uncertainties are taken from Ref. [10]; and the relative efficiency factors, ϵ, are obtained from simulations. Since the analysis starts from a given number of selected $D^+_{(s)} \to \pi^+\pi^+\pi^-$ decays, there are no normalisation channels.

5. Event selection

The event selection comprises an initial stage in which relatively loose criteria are applied to select samples of candidate $D^+_{(s)} \to \pi^+\pi^+\pi^-$ decays. A boosted decision tree (BDT) [11] is then used to further suppress backgrounds. Candidate $D^+_{(s)} \to \pi^+\pi^+\pi^-$ decays are required to have three good quality, high-p_{T} tracks consistent with coming from a vertex that is displaced from any primary vertex (PV) in the event, by typically 150 μm (300 μm) for D^+ (D^+_s). Loose particle identification criteria are applied, requiring the tracks to be consistent with the pion hypothesis. The three-track system is required to have total charge $\pm e$, its invariant mass must be in the range 1820–2020 MeV/c^2, and its combined momentum vector must be consistent with the direction from a PV to the decay vertex. The invariant mass of opposite-sign candidate pion pairs is required to be in the range 300–1650 MeV/c^2; this removes backgrounds where a random

pion is associated with a vertex from either a $\gamma \to e^+e^-$ conversion, in which both electrons are misidentified as pions, or from a $D^0 \to K^-\pi^+$ decay, where the kaon is misidentified as a pion. The BDT has six input variables for each of the tracks, together with three variables related to the quality of the decay vertex and the association of the $D^+_{(s)}$ candidate with the PV. The track variables are related to track fit quality, particle identification probabilities and the quality of the track association to the decay vertex. The cut value of the BDT and the signal mass window are then selected by a bidimensional optimisation of the statistical significance of the $D^+_{(s)}$ signal. Figure 1 shows the $\pi^+\pi^+\pi^-$ mass spectra for Runs 1 and 2, before and after the BDT selection. The discontinuity in the Run 2 spectrum comes from the fact that the trigger has two separate output streams and there are different BDT cuts for D^+ and D^+_s. The yield per fb^{-1} is larger in Run 2 than in Run 1 by a factor 3.3, arising from the larger cross-section [12], and from a higher trigger efficiency for charm.

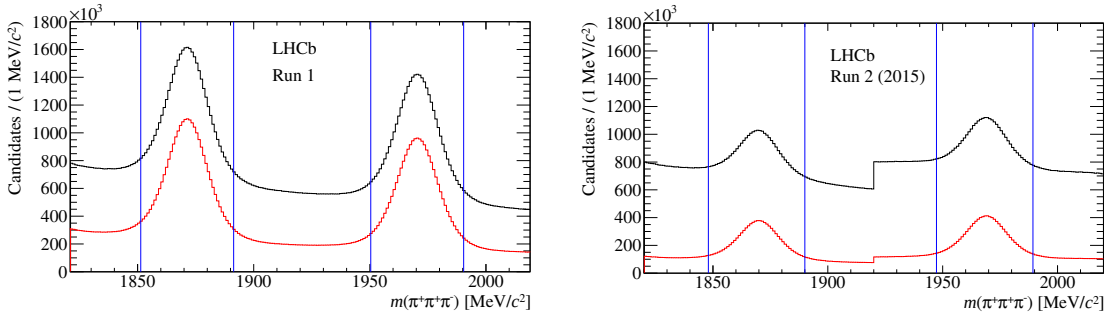

Figure 1: Three pions invariant mass before (black) and after (red) the BDT selection, for Run 1 (left) and Run 2 (right). The vertical lines define the optimised mass windows. Figures from [8].

6. Fits to the $\pi^+\pi^+\pi^-$ mass spectra

The BDT-selected events are fitted to extract the number of D^+ and D^+_s candidates. The background model comprises a fourth order Chebyshev polynomial for the combinatorial background and six shapes to account for sources of irreducible background, taken from high statistics simulations: one for $D^+_s \to K^+\pi^+\pi^-$, where the kaon is misidentified as a pion, one for $D^+_s \to \pi^+\pi^+\pi^-\pi^0$, where the π^0 is missing and four for $D^+_{(s)} \to (\eta^{(\prime)} \to \pi^+\pi^-\gamma)\pi^+$, where the photon is missing. The signal model is a sum of a Gaussian function and a double sided Crystal Ball function [13] for each of the two peaks. The fit results are shown in Figure 2. The total $D^+_{(s)} \to \pi^+\pi^+\pi^-$ signal yields in the optimised mass windows, summed over Run 1 and Run 2 data, are 2.49×10^7 for D^+ and 2.37×10^7 for D^+_s, with backgrounds of 1.38×10^7 and 1.08×10^7, respectively, within the same mass windows. Uncertainties of $\pm 2\%$ are assigned to each total yield to account for imperfections in the fits to the mass spectra.

7. Variation of efficiency as a function of $\pi^+\pi^-$ mass

The relative efficiency factors in Eq. 1 are obtained from simulation. Fully simulated $\pi^+\pi^-$ mass spectra from $D^+ \to \pi^+\pi^+\pi^-$ decays for Run 1 are divided by the generated spectra to give the relative efficiency as a function of the $\pi^+\pi^-$ mass. The efficiency is highest at large $\pi^+\pi^-$ masses, mainly due to the effects of the hardware and software triggers. The relative efficiencies in Run 1 data are found to be $\epsilon(\eta) = 0.85 \pm 0.01$ and $\epsilon(\eta') = 1.01 \pm 0.01$ for D^+ and $\epsilon(\eta) = 0.80 \pm 0.01$ and $\epsilon(\eta') = 1.03 \pm 0.01$ for D^+_s, where the uncertainties come from the simulation sample size. The relative efficiencies for Run 2 are found to be statistically compatible with those for Run 1, through a comparison of the $\pi^+\pi^-$ mass spectra from the D^+ and D^+_s signal candidates in the data. An additional systematic uncertainty of 2% is assigned to the Run 2 relative efficiencies, reflecting the statistical precision of the comparison.

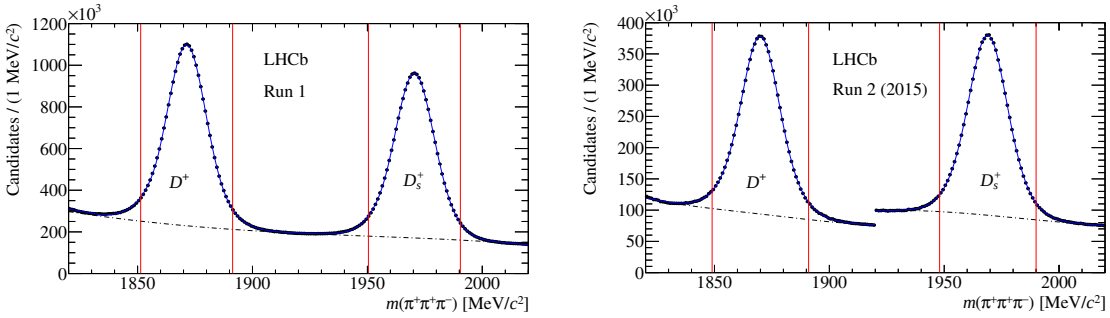

Figure 2: Fits to the $\pi^+\pi^+\pi^-$ invariant mass for Run 1 (left) and Run 2 (right). The black dashed line represents the sum of all background contributions. The vertical lines define the optimised mass windows. Figures from [8].

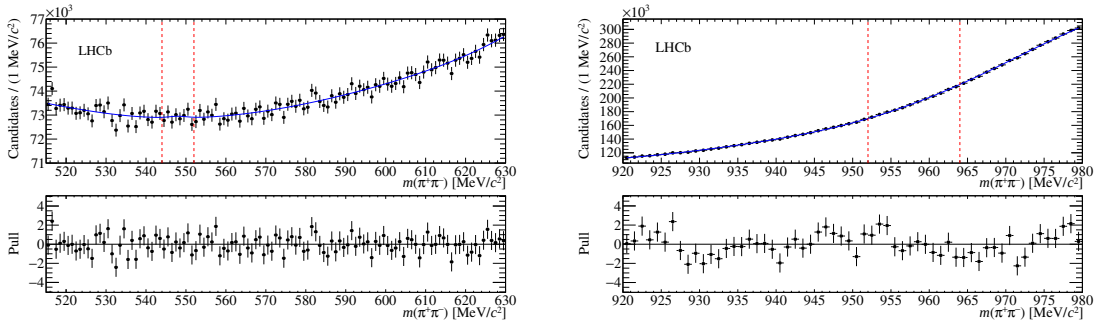

Figure 3: The $\pi^+\pi^-$ invariant mass distribution in the η (left) and η' (right) mass fitting region from the sum of the four samples, showing also the sum of the fitted curves and the pulls. The vertical dashed lines indicate the respective signal regions. Figures from [8].

8. Mass spectra for $\pi^+\pi^-$

For each of the η and η' resonances there are four separate $\pi^+\pi^-$ mass spectra, from the D^+ and the D_s^+ for each of Runs 1 and 2. Figure 3 shows the sums of the four $\pi^+\pi^-$ mass spectra for the η and η' mass fitting ranges. The vertical dashed lines indicate the signal regions, which cover the intervals 544–552 MeV/c^2 for the η and 952–964 MeV/c^2 for the η', in each case approximately ± 2 times the $\pi^+\pi^-$ mass resolution; they have been kept blind until the end of the analysis optimisation. The resolution is calculated from a dedicated $D^+ \to (\eta^{(\prime)} \to \pi^+\pi^-)\pi^+$ Monte Carlo sample, and cross-checked using $K^0_s \to \pi^+\pi^-$ decays in data. The resolution from Monte Carlo and the one from data are found to be consistent and the difference is assigned as a systematic error. The mass resolutions are found to be $\sigma_\eta = 2.2 \pm 0.1$ MeV/c^2 and $\sigma_{\eta'} = 2.7 \pm 0.1$ MeV/c^2.

9. Systematic uncertainties

Several sources of systematic uncertainties are considered: errors on the branching fractions used in Equation 1, errors on the fitted numbers of D^+ and D_s^+ (dominated by the variation of the residuals), uncertainty in the variation of the relative efficiency, uncertainty in the extracted background PDF and in the dipion mass resolution. They are found to have no effect on the results, which are dominated by the statistical uncertainties; the systematic uncertainties together account for about 1% of the total uncertainty.

10. Limit setting

Since there is no evidence for any signal, the CL_s method [14] is used to obtain observed upper limits on the branching fraction. The signal PDFs are extracted by fitting a dedicated MC

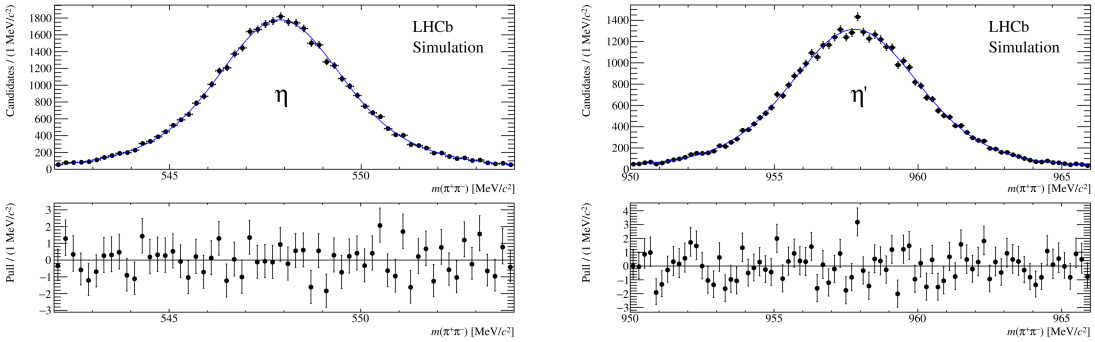

Figure 4: Mass spectra for $\eta \to \pi^+\pi^-$ (left) and $\eta' \to \pi^+\pi^-$ (right) from simulation, with the result of a fit to a double Gaussian function. Figures from [8].

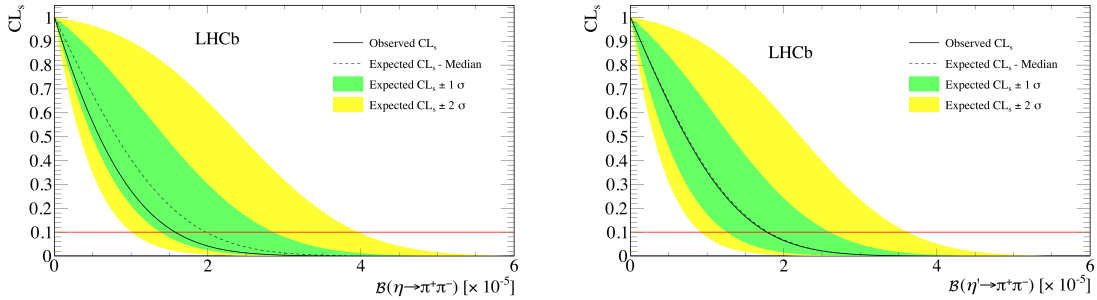

Figure 5: Values of CL_s as function of $\mathcal{B}(\eta \to \pi^+\pi^-)$ (left) and $\mathcal{B}(\eta' \to \pi^+\pi^-)$ (right). The horizontal line indicates the 90% confidence level. Figures from [8].

sample, and are shown in Figure 4. The background PDFs come from the fits shown in Figure 3. The profile likelihood ratio is used as test statistic. The results of the $\mathrm{CL_s}$ method are shown in Figure 5, along with the expected distribution. The observed limits at 90% CL are found to be $\mathcal{B}(\eta \to \pi^+\pi^-) < 1.6 \times 10^5$ and $\mathcal{B}(\eta' \to \pi^+\pi^-) < 1.8 \times 10^5$.

11. Conclusions

A new method is introduced to search for the decays $\eta \to \pi^+\pi^-$ and $\eta'(958) \to \pi^+\pi^-$, which would violate *CP* symmetry in the strong interaction. The method relies on the copious production of charm mesons at LHCb, and will improve in sensitivity as more data are collected at the LHC. With the LHC Run 1 data and data from the first year of Run 2, the limit obtained on the branching fraction for the decay $\eta \to \pi^+\pi^-$ is comparable to the existing limit, while that for $\eta' \to \pi^+\pi^-$ is a factor three better than the previous limit.

References

[1] H.-Y. Cheng, *The strong CP problem revisited*, Phys. Rept. **158** (1988) 1.
[2] R. Jackiw and C. Rebbi, *Vacuum periodicity in a yang-mills quantum theory*, Phys. Rev. Lett. **37** (1976) 172.
[3] C. G. Callan, Jr. R. F. Dashen, and D. J. Gross, *The Structure of the Gauge Theory Vacuum*, Phys. Lett. **B63** (1976) 334.
[4] J. Kuckei *et al.*, *Strong CP violation and the neutron electric dipole form factor*, Phys. Atom. Nucl. **70** (2007) 349, `arXiv:hep-ph/0510116`.
[5] C. Jarlskog and E. Shabalin, *How large are the rates of the CP violating $\eta, \eta' \to \pi\pi$ decays?*, Phys. Rev. **D52** (1995) 248.
[6] KLOE collaboration, F. Ambrosino *et al.*, *Upper limit on the $\eta \to \pi^+\pi^-$ branching ratio with the KLOE detector*, Phys. Lett. **B606** (2005) 276, `arXiv:hep-ex/0411030`.
[7] BESIII collaboration, M. Ablikim *et al.*, *Search for CP and P violating pseudoscalar decays into $\pi\pi$*, Phys. Rev. **D84** (2011) 032006, `arXiv:1106.5118`.

[8] LHCb collaboration, R. Aaij *et al.*, *Search for the CP-violating strong decays* $\eta \to \pi^+\pi^-$ *and* $\eta'(958) \to \pi^+\pi^-$, arXiv:1610.03666.
[9] R. Aaij *et al.*, *Tesla : an application for real-time data analysis in High Energy Physics*, Comput. Phys. Commun. (2016) , arXiv:1604.05596.
[10] Particle Data Group, K. A. Olive *et al.*, *Review of particle physics*, Chin. Phys. **C38** (2014) 090001, and 2015 update.
[11] B. P. Roe *et al.*, *Boosted decision trees as an alternative to artificial neural networks for particle identification*, Nucl. Instrum. Meth. **A543** (2005) 577, arXiv:physics/0408124.
[12] LHCb collaboration, R. Aaij *et al.*, *Measurements of prompt charm production cross-sections in pp collisions at* $\sqrt{s} = 13$ *TeV*, JHEP **03** (2016) 159, arXiv:1510.01707.
[13] T. Skwarnicki, *A study of the radiative cascade transitions between the Upsilon-prime and Upsilon resonances*, PhD thesis, Institute of Nuclear Physics, Krakow, 1986, DESY-F31-86-02.
[14] A. L. Read, *Presentation of search results: The* CL_s *technique*, J. Phys. G: Nucl. Part. Phys. **28** (2002) 2693.